frontiers | Frontiers in Earth Science

ORIGINAL RESEARCH
published: 10 May 2022
doi: 10.3389/feart.2022.899947

Paleo-Environmental Variation and Its Control on the Organic Matter Accumulation in Black Shale of the Permian Gufeng Formation in the Lower Yangtze Area, South China

Weibing Shen[1], Yangyang Wang[2], Ziyu Zheng[3], Shihao Shen[4], Hongzhe Xie[1], Haoyi Qin[1] and Maquzong Bai[1]*

[1]MNR Key Laboratory of Isotope Geology, MNR Key Laboratory of Deep-Earth Dynamics, Institute of Geology, Chinese Academy of Geological Sciences, Beijing, China, [2]National Institute of Natural Hazards, Ministry of Emergency Management of China, Beijing, China, [3]Liaohe Geophysical Exploration Company Branch, BGP, CNPC, Liaoning, China, [4]Geological Survey of Anhui Province, Hefei, China

OPEN ACCESS

Edited by:
Kun Zhang,
Southwest Petroleum University, China

Reviewed by:
Daxiang He,
Yangtze University, China
Hexin Huang,
Chang'an University, China
Xinjian Zhu,
PetroChina Hangzhou Research Institute of Geology, China

***Correspondence:**
Yangyang Wang
wyy871217@126.com

Specialty section:
This article was submitted to Geochemistry, a section of the journal Frontiers in Earth Science

Received: *19 March 2022*
Accepted: *06 April 2022*
Published: *10 May 2022*

Citation:
Shen W, Wang Y, Zheng Z, Shen S, Xie H, Qin H and Bai M (2022) Paleo-Environmental Variation and Its Control on the Organic Matter Accumulation in Black Shale of the Permian Gufeng Formation in the Lower Yangtze Area, South China. Front. Earth Sci. 10:899947. doi: 10.3389/feart.2022.899947

Mechanism of the organic matter (OM) accumulation in the Middle Permian Gufeng Formation shale in South China is lack of constraints, which restricts the source rock evaluations and shale gas explorations. To decipher the OM accumulation of the Gufeng Formation, geological and geochemical results related to paleo-environmental variations are presented from the shelf Putaoling section in South China. The OM accumulation in the Gufeng Formation is vertically heterogeneous, shown by a medium total organic carbon (TOC) content (2.3%) in the lower member and a high TOC content (9.6%) in the upper member. The organic-rich shales of the Gufeng Formation are deposited in a complex paleo-environment with restrained water conditions, a warm and humid paleoclimate, a relatively strong chemical weathering, significant hydrothermal activities, a high primary productivity, fluctuating redox conditions, and a relatively high sedimentary rate. Compared to the lower member deposited under anoxic conditions, the upper member is formed in a dominantly euxinic environment with higher productivities. The seawater deoxygenation and the upward-increasing productivity jointly lead to the vertical heterogeneity of the OM accumulation in the Gufeng Formation. Thus, an 'integrated model' for the OM accumulation in the Gufeng Formation is established, and which adds to our knowledge that no a single factor or model can explain the OM accumulation in all sedimentary environments.

Keywords: South China, shale gas, redox state, primary production, OM accumulation, Permian

1 INTRODUCTION

The Middle Permian (Guadalupian; Clapham, 2015) witnesses a separate extinction event, a large igneous province, and a global cooling event (Jin et al., 1994; Retallack et al., 2006; Montanez et al., 2007; Wignall et al., 2009; Bond et al., 2010a; 2010b), which represents a critical time in the Earth history. During this time, a set of organic-rich deposits is worldwide developed, representing one of the most important periods for the hydrocarbon source rock formation (Kametaka et al., 2005; Large

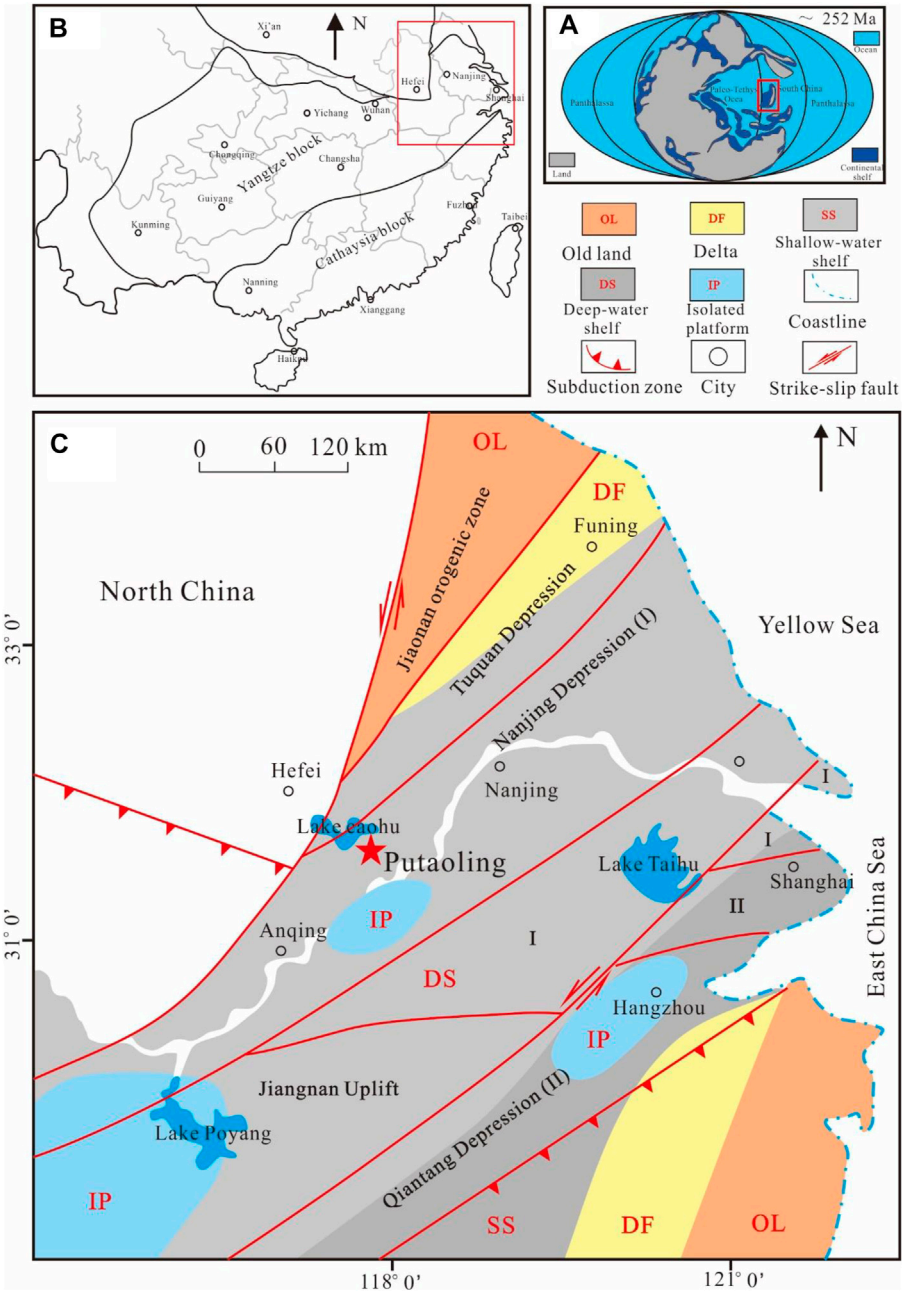

FIGURE 1 | (A) Late Guadalupian palaeogeography and the relative location of South China [modified from Liu and Selby (2021)]. **(B)** Tectonic division map of South China and the location of the Lower Yangtze area. **(C)** Location map of the studied area showing the middle Permian tectonic units and facies distribution. The sampling Putaoling section can be seen [modified from Bai et al. (2021) and Ding et al. (2021)].

et al., 2015; Zhang et al., 2019). With the acceleration of 'petroleum exploration near the source' in the petroleum industry, the Middle Permian organic-rich deposits and their hosted unconventional hydrocarbon resources attract more and more attentions in the Lower Yangtze area, South China.

In recent years, a lot of investigations have been carried out on the sedimentary environment, reservoir characteristics, source rock quality, and potential evaluation of the shale gas resource in the Middle Permian organic-rich shale in the Lower Yangtze area (Takebe et al., 2007; Du et al., 2015; Fu et al., 2021). The results generally propose that the Middle Permian shale has a large thickness, a high organic carbon content, a moderate maturity, good gas-bearing conditions, and a large potential of shale gas resources (Ma et al., 2009; Du et al., 2015; Zhao et al., 2020; Fu et al., 2021; Bolin Zhang et al., 2020). However, the mechanism of the OM accumulation in the Middle Permian shale is rare. In particular, studies have deducted that the OM would affect the hydrocarbon generation capacity, pore structures, and adsorption

characteristics of organic sediments, which play a decisive role in the shale gas content (Huang et al., 2020; Huang et al., 2021; Kun Zhang et al., 2020; Zhang et al., 2022a; Zhang et al., 2022b; Zhang et al., 2022c). The mechanism of the OM accumulation in shales is gradually reaching a consensus, that is, the paleo-environment, including the primary productivity (Gallego-Torres et al., 2007) and preservation conditions (Mort et al., 2007; Kennedy et al., 2014), determines the accumulation of the OM (Ibach, 1982; Pedersen and Calvert, 1990; Arthur and Sageman, 1994; Murphy et al., 2000; Sageman et al., 2003; Rimmer et al., 2004; Ding et al., 2021). Thus, to further understand the shale gas enrichment in the Middle Permian shale in the Lower Yangtze area, the sedimentary environment for the shale formation and its control on the OM enrichment in the shale should be investigated in detail.

This study, taking the Gufeng Formation in the shelf Putaoling section as an example, carries out a detailed investigation on the Middle Permian shales in the Lower Yangtze area, South China. Lithology and geochemistry (TOC and elements) records are employed to perform the objectives. The main objectives of the study are 1) to construct the paleo-environment of the Middle Permian period and 2) to reveal the mechanism of OM accumulation in the Gufeng Formation shale.

2 GEOLOGICAL SETTING AND SECTION DESCRIPTION

During the Middle–Late Permian, the South China plate, located near the ancient equator, was adjacent to the ancient Tethys Ocean in the west and the Panthalassic Ocean in the east (**Figure 1A**; Liu and Selby, 2021). The Lower Yangtze area lies in the present northeastern South China and can be divided into two major tectonic units: the Jiangsu-Anhui tectonic belt and the Jiangnan uplift belt (**Figure 1B**; Ding et al., 2021). The Jiangsu-Anhui tectonic belt is characterized by a continuous subsidence and consists of the Nanjing Depression, the Tuquan Depression, and the Jiaonan orogenic zone, whereas the Jiangnan uplift belt, mainly feathered with the weathering and denudation, is composed of the Jiangnan Uplift and the Qiantang Depression (**Figure 1C**; Ding et al., 2021). Based on the previous studies (e.g., Ma et al., 2009), the Lower Yangtze area, during the Middle–Late Permian, experienced a regional uplift, leading to an evident retroregression and the formation of continental-marine transition facies. Accordingly, a set of marine shale and transitional clastic rock strata, including the Middle Permian Qixia Formation and Gufeng Formation, as well as the Upper Permian Longtan Formation and Dalong Formation, was deposited (Ma et al., 2009). During the deposition of the Gufeng Formation, the northern and southeastern Lower Yangtze areas were paleo-continents, and the central part of which was deep-water shelf to shelf facies. Particularly, the deep-water shelf to shelf facies gradually transitioned to delta facies toward to the southeast and northern paleo-continents (**Figure 1C**; Bai et al., 2021).

The study section—Putaoling section—is located in the Jiangsu-Anhui tectonic belt of the Lower Yangtze area (**Figure 1C**). The exposed strata, from bottom to top, are the Carboniferous Chuanshan Formation, Permian Qixia Formation, Gufeng Formation, Longtan Formation, and Dalong Formation, as well as the Triassic Yinkeng Formation (**Figure 2**). The Permian Gufeng Formation at the Putaoling section, about 32.9 m thick, is mainly composed of organic-rich black siliceous shales and characterized by a complete sedimentary cycle with a sea level rising and falling (**Figure 2B**). According to regional sea level fluctuations, the Gufeng Formation can be generally divided into two members (**Figure 2B**): 1) The lower member conformable contacts with the underlie Qixia Formation and predominantly consists of black siliceous shales and carbonaceous shales, with thin silty mudstone intervals and a decreasing-upward silica contents. This member is deposited in the shallow-water shelf facies. 2) The upper member conformable contacts with the overlie Longtan Formation and is dominated by black siliceous shales and siliceous carbonaceous shales, with horizontal beddings and abundant pyrite/phosphorite nodules. This member is a set of deep-water shelf deposition.

3 SAMPLE AND METHODS

3.1 Sample Collection

In this study, a total of 22 fresh shale samples, including 7 samples from the lower member and 15 samples from the upper member, are collected from the Gufeng Formation. To ensure sampling accuracy, a surface layer with a thickness of approximately 0.3 m is removed to avoid the interference from weathering. The details for the sample No., depths, and lithofacies are shown in **Figure 2B**. Positioned according to the distance from the strata boundaries, samples are collected at a maximum spacing of 2–3 m in the Gufeng Formation. After removing the outer epidermis in the laboratory, all of the samples are ground to 200 mesh by hand under pollution-free conditions.

3.2 Experimental Methods

The analysis and test for the major, trace, rare elements and TOC are all performed at the National Research Center for Geoanalysis, China.

To remove carbonate minerals, an appropriate amount of 10% HCl is used to dissolve the powdered samples (about 0.5 g). The residue is washed with the ultrapure water and then dried in a desiccator for 10 h at 60°C, followed by a combustion at 900°C to oxidize organic carbon in a pure oxygen atmosphere. The resultant carbon dioxide is subsequently measured to provide the TOC data. The testing instrument is a LECO CS-230 carbon analyzer.

About 1.0 g powder samples are used to analyze the major elements. The weighted samples are mixed with the 130 mg (ratio about 1:4) anhydrous lithium metaborates in a 10 ml graphite pot. After that, the mixture is melted for 15 min at 1000°C, and the molten substance is poured into 5% aqua regia for a complete dissolution. Then the solution, with the addition of accurately 25 μL 1 mg/ml cadmium standard solutions, is transferred into a 25 ml colorimetric tube. Finally, the 5% aqua regia is used to dilute the mixed liquor. The content of elements is measured by a

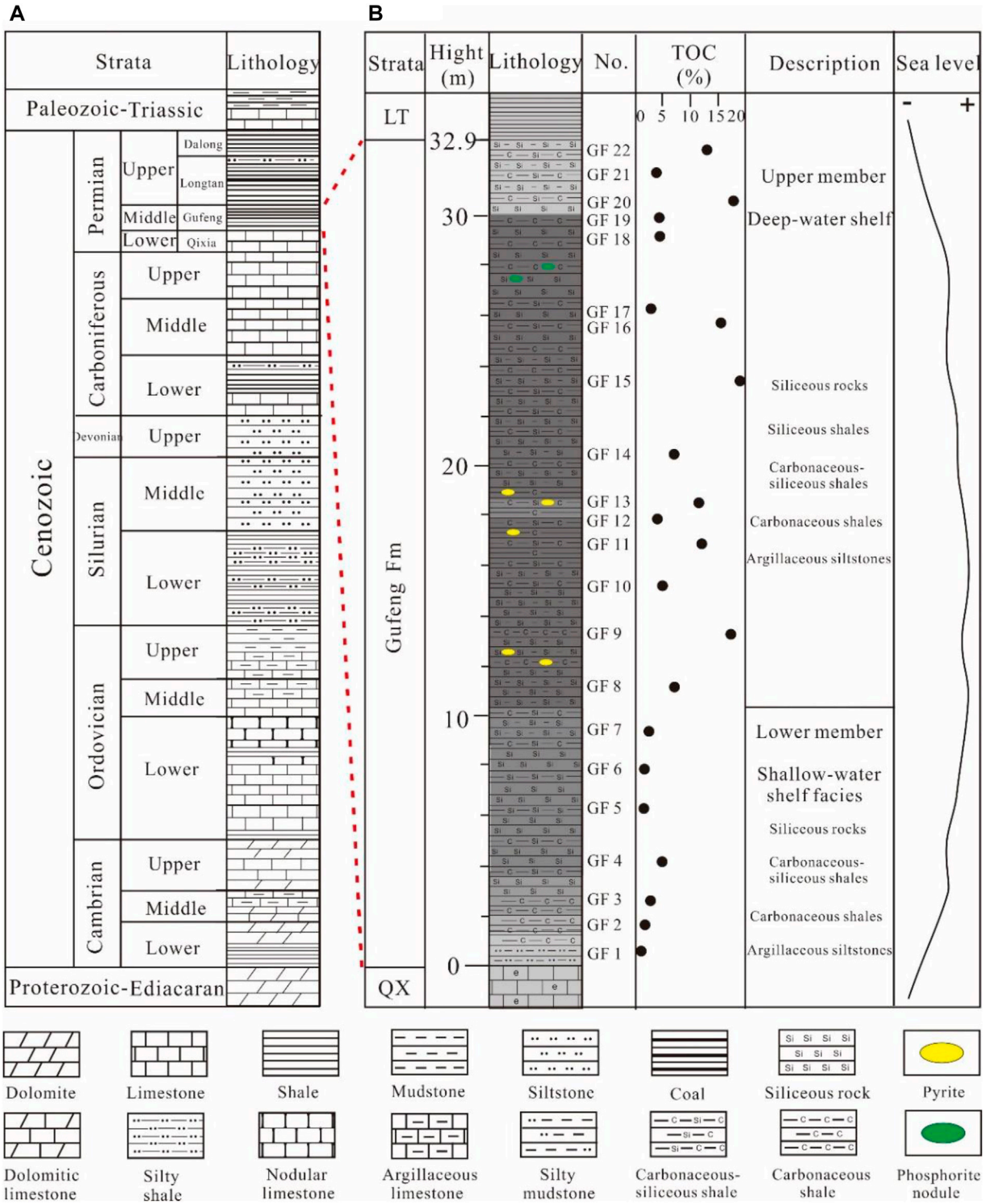

FIGURE 2 | Stratigraphic log **(A)** in the Lower Yangtze area and the stratigraphic column **(B)** of the Gufeng Formation at the Putaoling section. QX, Qixia Formation; LT, Longtan Formation.

ICP-AES, and the precision is RSD <2% ~ 8%. For the trace element and rare earth element (REE) analysis, about 25 mg samples are weighed into a Teflon vessels with a steel jacket. The hydrofluoric acid and nitric acid are added to dissolve the samples at 190°C for 48 h. Then the cooled solution is dried on an electric heating plate, and the precipitates are re-dissolved with the

hydrochloric acid for 3 h. Finally, the solution is transferred into a clean centrifugal tube for testing. The samples are tested by an inductively coupled plasma mass spectrometry, and the method precision is (RSD) < 10%.

3.3 Data Processing

Element accumulation factors (EFs) are calculated from X_{EF} = [(X/Al) $_{sample}$/(X/Al) $_{PAAS}$] (Calvert and Pedersen, 1993), where the element contents of PAAS are referred to the Taylor and McLennan, 1985). Chemical index of alteration (CIA) is calculated from CIA = [Al_2O_3/(Al_2O_3 + CaO* + Na_2O+ K_2O)] × 100, where the oxides are in a mole fraction, and the CaO* represents the CaO content in silicate (Fedo et al., 1995). Mclennan (1993) proposes a method to calculate and calibrate the CaO*. If the number of moles of the (CaO-10/3P_2O_5) is less than that of the Na_2O, the (CaO-10/3P_2O_5) value is taken as the CaO* value. On the contrary, it takes the mole number of the Na_2O as the mole value of the CaO*.

4 RESULT

4.1 TOC

The Gufeng Formation contains abundant OM, and its TOC contents range from 1.1% to 18.9%, with an average of 7.3%. Vertically, the OM accumulation in the shales of the Gufeng Formation is evidently heterogeneous (**Figure 2**): The black siliceous shales and carbonaceous shales in the lower member have relatively lower TOC contents (less than 5%), whereas the black siliceous shales and siliceous carbonaceous shales in the upper member have larger TOC contents, with an average of 9.6% (up to 18.9%) (**Figure 2**).

4.2 Element

4.2.1 Major Element

The major elements, expressed as the oxides, are dominated by SiO_2, Al_2O_3, and CaO. The w (SiO_2) of the Gufeng Formation is the largest (77.9 ± 11.6%). It is higher than 62.8% of the Late Archean shale of Australia. The w (Al_2O_3), w (CaO), w (K_2O), and w (P_2O_5) are successively followed, and they are 4.6 ± 2.7%, 1.1 ± 2.4%, 0.71 ± 0.54%, and 0.66 ± 1.80%, respectively. The stratigraphic distributions of the w (SiO_2), w (Al_2O_3), and w (CaO) are relatively stable in the Gufeng Formation, whereas the w (P_2O_5) have vertical variations. In particular, the w (P_2O_5) first decreases and then increases from bottom to top.

4.2.2 Trace Element

Compared with the standard values of the PAAS, the trace elements, such as Mo, U, V, Ni, Cd, Zn, and Cr, in the Gufeng Formation show enrichments. For example, the contents of Mo (89.5 ± 73.5 μg/g), U (16.9 ± 20.3 μg/g), and V (902.1 ± 587.8 μg/g) are large. However, Co, Pb, and Sc are depleted in most samples of the Gufeng Formation. Compared to the lower member, the contents of some trace elements in the upper member are evidently higher, and the Mo_{EF} and U_{EF} can be up to 1,000.

4.2.3 Rare Earth Element

Concentrations of REE (ΣREEs) in the Gufeng Formation range from 36.96 μg/g to 556.5 μg/g, with an average of 131.1 μg/g. The

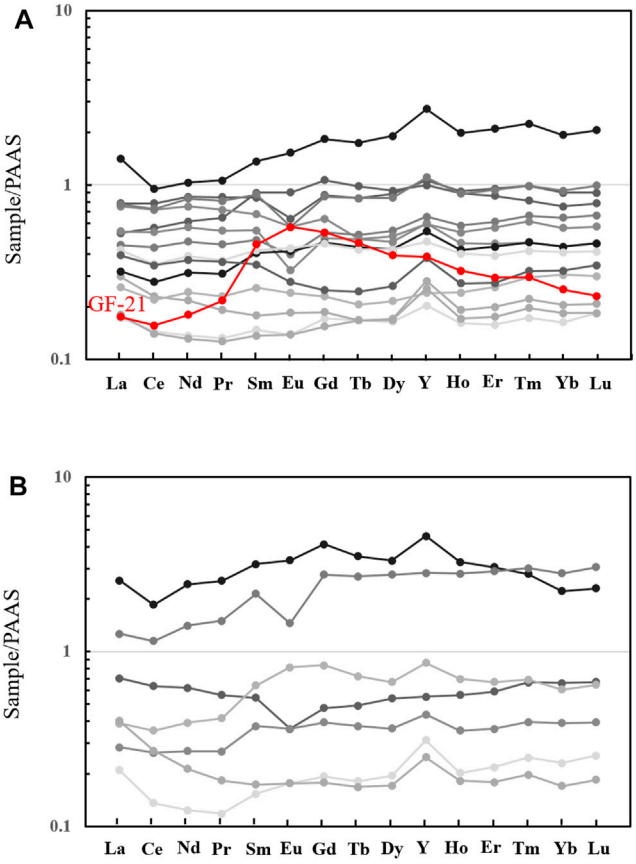

FIGURE 3 | PAAS-normalized REE patterns of the shale samples from the Permian Gufeng Formation at the Putaoling section. **(A)** and **(B)** are the upper member and lower member, respectively.

ΣREEs are significantly lower than 185 μg/g of the PAAS, showing the REE depletion in the Gufeng Formation. The PAAS-normalized REE distribution patterns of the upper and lower members of the Gufeng Formation are similar, and they are relatively flat (**Figure 3**). For the samples from the lower member, the PAAS-normalized REE distribution patterns are characterized by slight left-leaning, shown by slightly negative Ce anomalies (Ce/Ce* = $Ce_N/(La_N \times Pr_N)^{1/2}$), insignificantly positive Eu anomalies (Eu/Eu* = $Eu_N/(Sm_N \times Gd_N)^{1/2}$), and obviously positive Y anomalies. Similarly, the PAAS-normalized REE distribution patterns of the samples from the upper member show slightly left-leaning, with obviously positive Y anomalies and higher Eu anomalies than those in the lower member. Notably, the upper member is highlighted by the sample GF21, which has an evident left-leaning pattern with a low LREE/HREE ratio and a significantly positive Eu anomaly (**Figure 3**).

5 DISCUSSION

5.1 Sedimentary Rate

The sedimentary rate has a significant effect on the OM accumulation (Murphy et al., 2000). Generally, the higher

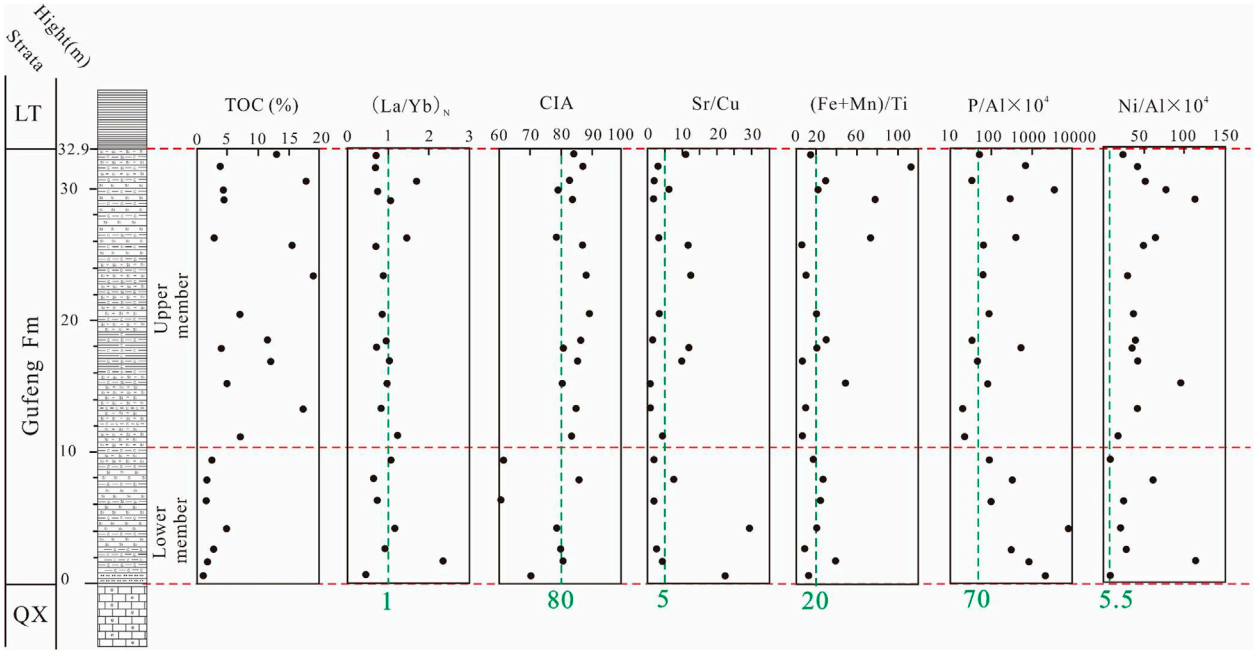

FIGURE 4 | Profiles of TOC, $(La/Yb)_N$, CIA, Sr/Cu, (Fe + Mn)/Ti, P/Al, and Ni/Al from the shale samples in the Gufeng Formation at the Putaoling section. QX, Qixia Formation; LT, Longtan Formation.

sedimentary rate, by reducing the oxidative decomposition and biological consumption of the OM, is more conducive to the OM enrichment (Ibach, 1982; Ding et al., 2018). The REE distribution patterns and (La/Yb)N ratios can be used to evaluate the sedimentary rate (Murray et al., 1991; Cao et al., 2018): When the REE fractionation is weak and the (La/Yb)N ratios are close to 1.0, it reflects a short time for the REE attaching with the clay minerals and corresponds to a high sedimentary rate. When the REE fractionation is strong and (La/Yb)N ratios are significantly higher than or lower than 1.0, it reflects a long time for the REE attaching with the clay minerals and corresponds to a low sedimentary rate (Murray et al., 1991; Cao et al., 2018). The PAAS-normalised REE distribution patterns of the samples from the Gufeng Formation are flat, and the REE fractionations are weak (**Figure 3**), indicating a relatively stable sedimentary rate. Particularly, the (La/Yb)N ratios of the 22 rock samples range from 0.45 to 2.35, with an average of 0.99 (**Figure 4**), suggesting that the sedimentary rate is high during the deposition of the Gufeng Formation.

5.2 Paleo-Climate

CIA is an effective indicator for the quantitative analysis of the paleoclimate and its associated chemical weathering in the study area (Nesbitt and Young, 1982). Generally, CIA values are ~80–100 in strong chemical weathering areas with a hot and humid climate, ~60–80 in moderate chemical weathering areas with a warm and wet climate, and <60 in weak chemical weathering areas with a cold and dry climate (Nesbitt and Young, 1982; Young, 2002). The CIA values of the Gufeng Formation range from 60.4 to 89.4, with an average of 80.9, and reflect a moderately-strongly chemical weathering environment with a warm and humid climate (**Figure 4**). Vertically, the CIA values of the Gufeng Formation gradually increase upward. For the lower member, the CIA values range from 60.4 to 86.1, with an average of 74.0, and indicate a moderately chemical weathering environment with a typical warm and wet climate. The CIA values in the upper member range from 78.6 to 89.4, with an average of 84.2, and suggest a strongly chemical weathering environment with a typical hot and humid climate (**Figure 4**). Another evidence for qualitatively evaluating the paleoclimate is that the Sr/Cu ratio: Sr/Cu ratios are 1.3 ~ 5 in a warm and humid climate, and >5 in an arid and hot climate. Generally, the Sr/Cu ratios in the Gufeng Formation are less than 5, indicating a warm and humid climate (**Figure 4**). The warm and humid climate traced by CIA and Sr/Cu ratios of the Gufeng Formation is usually formed near the equator, which is consistent with the palaeogeographic position of South China during the Permian (**Figure 1A**).

5.3 Hydrothermal Activity

Based on the field survey, multilayers of ash and volcanogenic bentonite, with a regional distribution, are reported in the Permian strata in the southern Anhui area and indicate that the volcanic activity and the associated hydrothermal fluid occur in the study area (Shen et al., 2011; Liao et al., 2016). (Fe + Mn)/Ti ratios are efficient indicators for tracing the hydrothermal activities. When the (Fe + Mn)/Ti ratio >20 ± 5, sediments are generally considered to be affected by a hydrothermal fluid (Chu et al., 2016). As presented in **Figure 4**, (Fe + Mn)/Ti ratios from most samples of the Gufeng Formation are higher than 20

(**Figure 4**), suggesting that the hydrothermal activity is frequent during the deposition of the Gufeng Formation. In particular, the (Fe + Mn)/Ti ratios in the lower member range from 8.7 to 39.4 (with an average of 21.4), indicating slightly or weakly hydrothermal activities. Whereas the (Fe + Mn)/Ti ratios in the upper member range from 5.7 to 113.3, with an average of 32.6, suggesting significantly hydrothermal activities (**Figure 4**).

The REE distribution pattern, Y/Ho ratio, Ce anomaly, and Eu anomaly are usually employed to distinguish hydrothermal and non-hydrothermal siliceous shales (Bolhar et al., 2004; Slack et al., 2007; Zhou et al., 2014; Yao et al., 2014): 1) Terrigenous clasts show a LREE enrichment, high ∑REEs, no significant La anomaly, and chondrite-like Y/Ho ratios; 2) modern seawater is characterized by a LREE depletion, low ∑REEs, positive Y and La anomalies, strongly negative Ce anomalies, no significant Eu anomalies, and high Y/Ho ratios; and 3) hydrothermal fluids are featured with LREE enrichments, low ∑REEs, significantly positive Eu anomalies, and the chondrite-like Y/Ho ratios. Based on the PAAS-normalized REE distribution patterns of the samples from the Gufeng Formation (**Figure 3**), both the LREE and HREE are severely depleted. Meanwhile, most of the samples show a slightly left-leaning pattern, presenting slightly negative Ce anomalies, significantly positive Y anomalies, and weakly negative/positive Eu anomalies. These characteristics are similar to the REE distribution patterns of hydrothermal plume particles and the modern deep seawater (Bolhar et al., 2004; Slack et al., 2007; Yao et al., 2014; Zhou et al., 2014), suggesting the combination of hydrothermal and hydrogenous inputs. In addition, there are some differences between the REE distribution patterns of the upper member and those of the lower member, which suggests variations of REE sources or sedimentary environments. It is worth emphasizing that the samples with larger (Fe + Mn)/Ti ratios at the top of the Gufeng Formation, such as GF21, GF18, and GF17, have abnormally low ∑REEs (**Figure 3**). The sample GF-21 is taken as an example: 1) The ∑REEs is only 48.6 μg/g, 2) the PAAS-normalized REE distribution pattern is typical left-leaning, and 3) a significantly positive Eu anomaly is observed. These reflect the strong influence of hydrothermal activities.

5.4 Paleo-Productivity

During the deposition of the Gufeng Formation, the warm and humid climate and the associated moderately-strongly chemical weathering, as well as the frequent hydrothermal activities, jointly deliver the seawater with abundant nutrients, which are essential for a paleo-productivity improvement (Shanks and Bischoff, 1977; Zhang et al., 2005; Hung et al., 2018). In particular, the upward-increasing chemical weathering and hydrothermal activity recorded in the Gufeng Formation may control the stratigraphic variations in the biological productivity. The paleo-productivity cannot be measured directly and is usually evaluated with the major element (such as P), trace elements (Ni and Zn), etc. (Tyrrell, 1999; Rimmer et al., 2004; Schenau et al., 2005; Tribovillard et al., 2006; Schoepfer et al., 2015). In this study, P/Al and Ni/Al ratios are adopted to qualitatively estimate the paleo-productivity. The P/Al values of the samples from the Gufeng Formation range from 0.002 to 0.82, with an average of 0.082 (**Figure 4**). It is significantly higher than 0.007 of the PAAS standard and indicates high biological productivities. In particular, phosphorite nodules and the maximal P/Al value (0.818) are observed at the top of the Gufeng Formation (**Figure 4**), reflecting the higher biological productivity during

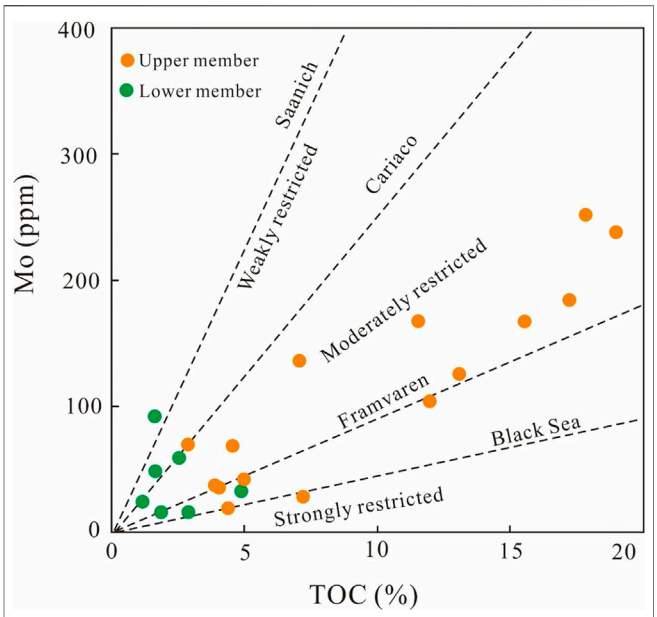

FIGURE 5 | Plot of the Mo concentration versus TOC from the shale samples in the Gufeng Formation at the Putaoling section. The dashed lines represent the regression trends for four modern marine systems (Saanich Inlet, Cariaco Basin, Framvaren Fjord, and Black sea), mirroring variable degrees of hydrographic restriction.

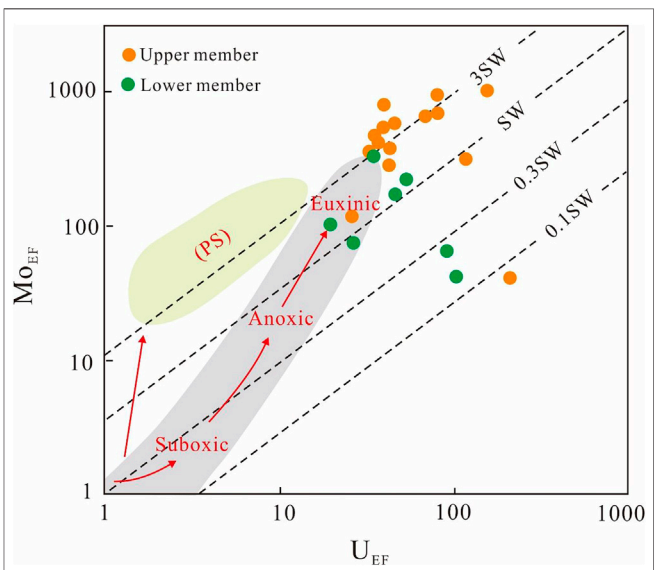

FIGURE 6 | Plot of the Mo_{EF} versus U_{EF} from the shale samples in the Gufeng Formation at the Putaoling section. PS = Particulate shuttle. The diagonal dotted lines represent different Mo/U ratios of modern seawater (0.1, 0.3, 1, and 3).

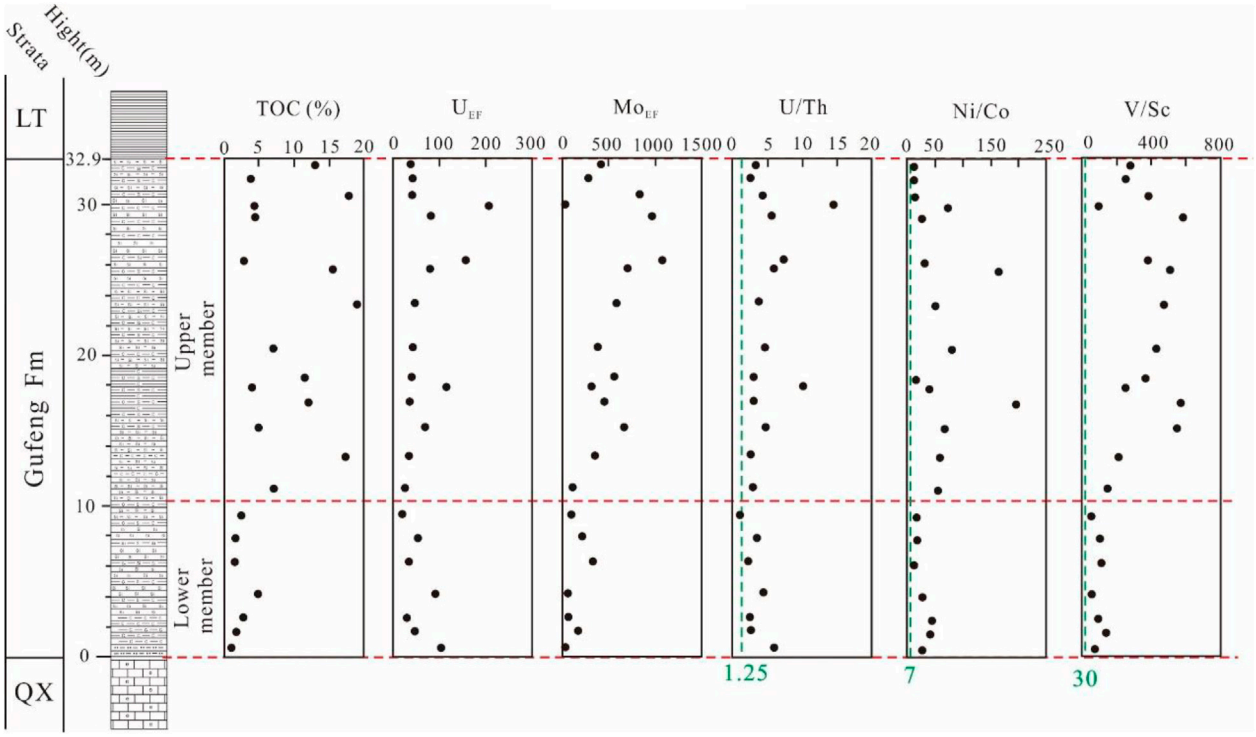

FIGURE 7 | Profiles of TOC, Mo_{EF}, U_{EF}, U/Th, Ni/Co, and V/Sc from the shale samples in the Gufeng Formation at the Putaoling section. QX, Qixia Formation; LT, Longtan Formation.

the deposition of the upper member. Similarly, the Ni/Al value of the samples from the Gufeng Formation is 0.0047 (**Figure 4**), which is significantly higher than 0.00055 of the PAAS standard. By comparison, the Ni/Al values of the lower member range from 0.0008 to 0.0112, with an average of 0.0037. The Ni/Al values of the upper member range from 0.0018 to 0.0112, with an average of 0.0052 (**Figure 4**). The stratigraphic variations of the paleo-productivity also are highlighted by the extremely high Ni/Al values at the top of the Gufeng Formation. These reflect an increasing-upward biological productivity in the Gufeng Formation.

5.5 Redox Conditions

Many redox indicators, such as sensitive trace element concentrations and their ratios, have been widely used to reconstruct redox conditions (Algeo and Tribovillard, 2009; Tribovillard et al., 2012). Before tracing the seawater redox state, hydrographic conditions to determine whether the Permian sea in South China is well connected with the open ocean should be investigated. The Mo-TOC diagram is an effective method to determine the water restriction conditions (Algeo and Lyons, 2006; Algeo and Rowe, 2012). As presented in **Figure 5**, the samples from the lower member fall in the weakly-moderately restricted field, similar to the modern Cariaco and Framvaren basins. The fluctuations of the weak and moderate water restrictions may be due to the regional sea level rising, which brings the eutrophic bottom current to exchange with the surface current. Whereas most of the samples from the upper member fall between those of the modern Framvaren Basin and Black Sea (**Figure 5**), suggesting moderately to strongly restricted water conditions. These show the increasing of the water restriction during the deposition of the Gufeng Formation.

Redox-sensitive metal elements (RSMs), such as Mo, U, and V, are usually enriched in anoxic conditions (Algeo and Tribovillard, 2009; Tribovillard et al., 2012). The V, Mo, and U are enriched in the lower member. Their contents range from 177 to 656 ppm, 15.3 to 91.7 ppm, and 3.78 to 55.7 ppm, with an average of 385.1, 41.3, and 19.7 ppm, respectively. The enrichments of the RSMs indicate anoxic conditions. For the upper member, V, Mo, and U contents range from 470 to 2130 ppm, 27.8 to 240.0 ppm, and 4.03 to 88.5 ppm, with an average of 1143.3, 112.0, and 15.7 ppm, respectively. The increase of the RSMs suggests a seawater deoxygenation. According to the U_{EF}-Mo_{EF} diagram (Algeo and Tribovillard, 2009; Tribovillard et al., 2012), all the samples from the lower member, with Mo_{EF} distributed between 65.2 and 340.8 with an average of 146.3, as well as U_{EF} distributed between 19.4 and 102.6 with an average of 53.2, fall in the anoxic field (**Figure 6**), whereas the samples from the upper member fall in the anoxic/euxinic region (**Figures 6**,**7**). In addition, the anoxic/euxinic conditions recorded in the upper member can be deducted from the enrichment of pyrite (**Figure 2**), which could be easily formed in the H_2S-rich environment (Lang et al., 2020). The TOC-Mo and U_{EF}-Mo_{EF} diagrams show that the lower member is formed in an anoxic environment with relatively well water circulation, while the upper member is deposited in an anoxic/euxinic environment with relatively strong water restriction.

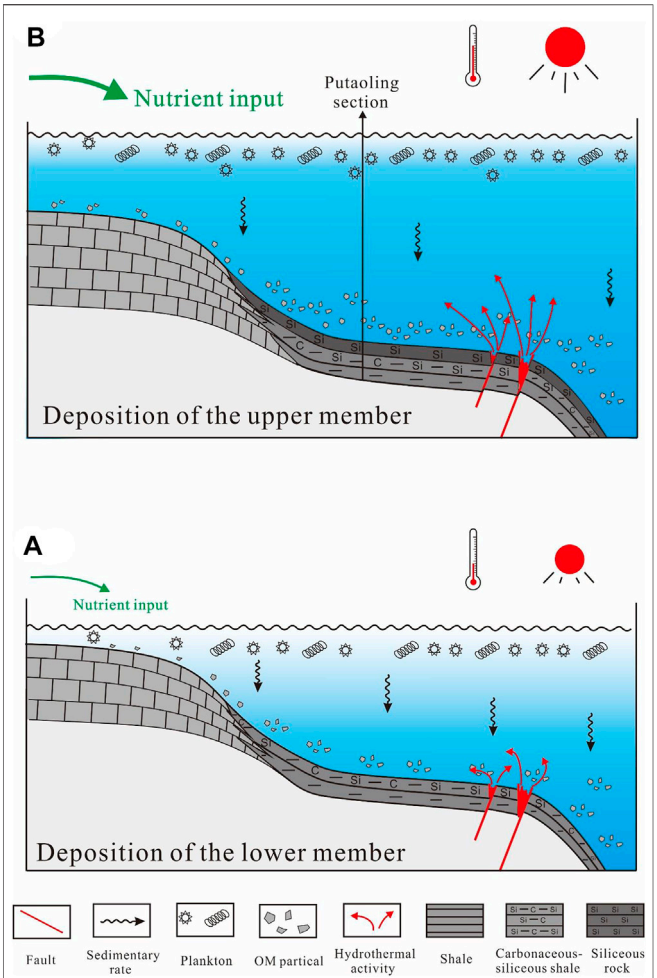

FIGURE 8 | Schematic diagram showing Permian climate, seawater redox state, distribution of black shale, hydrothermal activities, terrigenous input, and sedimentary rate in South China during **(A)** the deposition of the lower member and **(B)** the deposition of the upper member.

U/Th, Ni/Co, and V/Sc ratios are also effective indicators of the seawater redox conditions. Generally, the larger ratios reflect the higher degree of the seawater reduction (Hatch and Leventhal, 1992; Kimura and Watanabe, 2001; Algeo and Maynard, 2004; Rimmer, 2004; Canfield et al., 2008; Algeo and Tribovillard, 2009; Tribovillard et al., 2012): 1) The V/Sc ratios are <9 in oxic conditions, 9 ~ 30 in dysoxic conditions, and >30 in anoxic conditions; 2) the U/Th ratios are <0.75 in oxic conditions, 0.75 ~ 1.25 in dysoxic conditions, and >1.25 in anoxic conditions; and 3) the Ni/Co ratios are <5 in oxic conditions, 5 ~ 7 in dysoxic conditions, and >7 in anoxic conditions. The V/Sc, U/Th, and Ni/Co ratios of the samples from the lower member range from 54.3 to 136.2, from 0.9 to 5.9, and from 10.4 to 44.7, with an average of 87.3, 3.1, and 26.1, respectively (**Figure 7**). All of them indicate the anoxic conditions. Similarly, anoxic conditions recorded in the upper member are also shown by the V/Sc, U/Th, and Ni/Co ratios, which range from 93.9 to 208.2, from 2.8 to 14.4, and from 11.4 to 164.3, with an average of 363.8, 5.2, and 59.7, respectively (**Figure 7**). The increasing-upward V/Sc, U/Th, and Ni/Co ratios, as well as the Mo_{EF} and U_{EF}, indicate that the seawater deoxygenation occurs during the deposition of the Gufeng Formation.

5.6 Paleo-Environment Variation Controlling the OM Accumulation

The organic-rich siliceous shales of the Gufeng Formation in the Lower Yangtze area are deposited in a relatively restricted environment with a high biological productivity, high sedimentary rate, and dynamic redox state.

5.6.1 Primary Production Provides a Material Source for the OM Accumulation

During the deposition of the lower member, the volcanic hydrothermal activities are frequent in the Lower Yangtze area (Shen et al., 2011; Liao et al., 2016), and nutrients released from the hydrothermal fluids are carried into the slope and shelf by the upwelling (**Figure 8A**). At the same time, the climate is humid and warm and is favorable for the chemical weathering, resulting in an accumulation of nutrients in the shore of the continental shelf (**Figure 8A**). The abundant nutrients promote the prosperity of siliceous organisms such as algae and radiolarians, which is an important source for the OM accumulation in the lower member. The large P/Al and Ni/Al ratios of the lower member indicate high paleo-productivity and sufficient OM sources, leading to the high TOC (2.3%). During the deposition of the upper member, the climate becomes hot and humid, and the chemical weathering further enhances, leading to the increase of the terrigenous nutrient input (**Figure 8B**). Meanwhile, the (Fe + Mn)/Ti ratios show that the hydrothermal activity enhances, and the persistent upwelling brings a steady stream of nutrients to the slope and shelf, further promoting the biological flourishing (**Figure 8B**). The P/Al and Ni/Al ratios in the upper member are evidently larger than those in the lower part and show a significant increasing of the paleo-productivity (**Figure 3**). The increasing of the paleo-productivity and the resultant increasing OM source result in the formation of the upper member with higher TOC (9.6%).

5.6.2 Redox State and Sedimentary Rate Are Conducive to the OM Preservation

During the deposition of the lower member, the sea level rises regionally, and weakly-moderately restricted water conditions are observed. The redox indexes, including U/Th, Ni/Co, V/Sc, Mo_{EF}, and U_{EF}, indicate widespread anoxic conditions in the study area. The PAAS-normalized REE distribution patterns and the $(La/Yb)_N$ ratios show a high sedimentary rate (**Figure 8A**), which greatly shortens the OM exposure time in the degradation region (Ibach, 1982; Cao et al., 2018). These control the effective preservation of the OM and the formation of the organic-rich lower member. During the deposition of the upper member, the sea level slowly falls and the water becomes more restricted. With the living space of organisms decreasing, the OM such as biological debris in the bottom water column increases, and the oxygen consumption increases, leading to the seawater deoxygenation (**Figure 8B**). The resultant anoxic/euxinic conditions are verified by the higher Mo_{EF}, U_{EF}, U/Th,

Ni/Co, and V/Sc ratios. The moderately-strongly restricted anoxic/euxinic environment, where the bottom flows are lack and the replenishment of free oxygen is rare, is difficult to decompose the OM. Meanwhile, the high sedimentary rate shown by the $(La/Yb)_N$ ratios can also shorten the time for the OM degradation. These make that the OM buries and preserves rapidly, forming the upper member with higher TOC (**Figure 8B**).

5.6.3 OM Enrichment Model

The productivity and preservation jointly control the OM accumulation in the Gufeng Formation shale of the Lower Yangtze area, and the OM accumulation model is a combination of the traditional 'productivity model' and 'preservation model'. During the deposition of the lower member, the sedimentary environment is weakly-moderately restricted and anoxic, which is benefit for the OM preservation (**Figure 8A**). Meanwhile, the hydrothermal fluid delivers the seawater with abundant nutrients, which can be brought into the light-transmitting zone of the shallow-water area by the sea level rising. In addition, the warm and humid paleoclimate leads to an input of nutrients from the terrestrial chemical weathering. The nutrients significantly promote the proliferation of microorganisms in the surface water, resulting in the high primary productivity. The effective preservation conditions and the adequate material source control the OM enrichment in the lower member (**Figure 8A**). During the deposition of the upper member, the sea level falls slowly, the moderately-strongly restricted water conditions occur. The hydrothermal activities, combining with the enhanced chemical weathering, jointly control a significantly influx of nutrients, which further promotes the blooms of organisms and improves the primary production (**Figure 8B**). The greater productivity and the resultant higher sinking flux of the OM can intensify the consumption of the oxygen in the water column (Wei, et al., 2012; Ding et al., 2020), resulting in the formation of the euxinic conditions. The euxinic conditions create a positive feedback that there exists a more conducive environment to the preservation of OM. Thus, an 'integrated model' for the OM accumulation in the upper member can also be established (**Figure 8B**).

6 CONCLUSION

1) The Permian Gufeng Formation in South China is deposited in a restrained environment with a fluctuating redox state and a high sedimentary rate. In particular, redox proxies evidently show widespread anoxic conditions for the lower member deposition but a seawater deoxygenation for the upper member deposition.
2) A warm and humid paleoclimate and its associated chemical weathering, as well as significantly hydrothermal activities, are recorded in the Permian Gufeng Formation of South China. Particularly, the chemical weathering and hydrothermal activities gradually enhance from bottom to top, controlling the upward-increasing productivity in the Gufeng Formation.
3) OM accumulation in the Permian Gufeng Formation likely reflects the interaction of multiple factors, including the paleo-climate, redox conditions, hydrothermal activity, chemical weathering, and sedimentary rate. Thus, an 'integrated model' of the OM accumulation, emphasizing both the primary production and preservation conditions, is proposed.

DATA AVAILABILITY STATEMENT

The raw data supporting the conclusion of this article will be made available by the authors, without undue reservation.

AUTHOR CONTRIBUTIONS

WBS and YYW designed the project; WBS, YYW, and SHS did the fieldwork and collected samples; WBS and HZX performed geochemical analyses; YYW, ZYZ, and WBS interpreted the data. WBS, ZYZ, HYQ, and MQZB wrote the paper, with additional input from all the co-authors.

FUNDING

This study was funded by the China Geological Survey Project (DD20221649; DD20190002), the Key R&D Program of China (2019YFA0708404), and the Key Laboratory of Deep-Earth Dynamics of Ministry of Natural Resources (J1901-20-1). The authors are particularly grateful to Editor Kun Zhang and the reviewers for their constructive reviews and comments on the manuscript.

REFERENCES

Algeo, T. J., and Lyons, T. W. (2006). Mo-total Organic Carbon Covariation in Modern Anoxic marine Environments, Implications for Analysis of Paleoredox and Paleohydrographic Conditions. *Paleoceanography* 21 (1), 1–23. doi:10.1029/2004pa001112

Algeo, T. J., and Maynard, J. B. (2004). Trace–element Behavior and Redox Facies in Core Shales of Upper Pennsylvanian Kansas–type Cyclothems. *Chem. Geol.* 206 (3), 289–318. doi:10.1016/j.chemgeo.2003.12.009

Algeo, T. J., and Rowe, H. (2012). Paleoceanographic Applications of Trace-Metal Concentration Data. *Chem. Geology.* 324-325, 6–18. doi:10.1016/j.chemgeo.2011.09.002

Algeo, T. J., and Tribovillard, N. (2009). Environmental Analysis of Paleoceanographic Systems Based on Molybdenum–Uranium Covariation. *Chem. Geol.* 268 (3), 211–225. doi:10.1016/j.chemgeo.2009.09.001

Arthur, M. A., and Sageman, B. B. (1994). MARINE BLACK SHALES: Depositional Mechanisms and Environments of Ancient Deposits. *Annu. Rev. Earth Planet. Sci.* 22, 499–551. doi:10.1146/annurev.ea.22.050194.002435

Bai, L. H., Shi, W. Z., Zhang, X. M., Xu, X. F., Liu, Y., Yang, Y., et al. (2021). Characteristics of Permian Marine Shale and its Sedimentary Environment in Xuanjing Area, South Anhui Province, Lower Yangtze Area. *Earth Sci.* 46 (6), 2204–2217. doi:10.3799/dqkx.2020.372

Bolhar, R., Kamber, B. S., Moorbath, S., Fedo, C. M., and Whitehouse, M. J. (2004). Characterisation of Early Archaean Chemical Sediments by Trace Element Signatures. *Earth Planet. Sci. Lett.* 222 (1), 43–60. doi:10.1016/j.epsl.2004.02.016

Bolin Zhang, B., Yao, S., Mills, B. J. W., Wignall, P. B., Hu, W., Liu, B., et al. (2020). Middle Permian Organic Carbon Isotope Stratigraphy and the Origin of the Kamura Event. *Gondwana Res.* 79, 217–232. doi:10.1016/j.gr.2019.09.013

Bond, D. P. G., Hilton, J., Wignall, P. B., Ali, J. R., Stevens, L. G., Sun, Y., et al. (2010a). The Middle Permian (Capitanian) Mass Extinction on Land and in the Oceans. *Earth-Science Rev.* 102, 100–116. doi:10.1016/j.earscirev.2010.07.004

Bond, D. P. G., Wignall, P. B., Wang, W., Izon, G., Jiang, H.-S., Lai, X.-L., et al. (2010b). The Mid-capitanian (Middle Permian) Mass Extinction and Carbon Isotope Record of South China. *Palaeogeogr. Palaeoclimatol. Palaeoecol.* 292, 282–294. doi:10.1016/j.palaeo.2010.03.056

Calvert, S. E., and Pedersen, T. F. (1993). Geochemistry of Recent Oxic and Anoxic marine Sediments-Implication for the Geological Record. *Mar. Geol.* 113 (1–2), 67–88. doi:10.1016/0025-3227(93)90150-t

Canfield, D. E., Poulton, S. W., Knoll, A. H., Narbonne, G. M., Ross, G., Goldberg, T., et al. (2008). Ferruginous Conditions Dominated Later Neoproterozoic Deep-Water Chemistry. *Science* 321, 949–952. doi:10.1126/science.1154499

Cao, J., Yang, R., Yin, W., Hu, G., Bian, L., and Fu, X. (2018). Mechanism of Organic Matter Accumulation in Residual Bay Environments: The Early Cretaceous Qiangtang Basin, Tibet. *Energy Fuels and Fuels* 32 (2), 1024–1037. doi:10.1021/acs.energyfuels.7b02248

Chu, C. L., Chen, Q. L., and Zhang, B. (2016). Influence on Formation of Yuertusi Source Rock by Hydrothermal Activities at Dongergou Section, Tarim Basin. *Acta Sedimentologica Sinica* 34 (4), 803–810. doi:10.14027/j.cnki.cjxb.2016.04.020

Clapham, M. E. (2015). Ecological Consequences of the Guadalupian Extinction and its Role in the Brachiopod-Mollusk Transition. *Paleobiology* 41, 266–279. doi:10.1017/pab.2014.15

Ding, J., Zhang, J., Tang, X., Huo, Z., Han, S., Lang, Y., et al. (2018). Elemental Geochemical Evidence for Depositional Conditions and Organic Matter Enrichment of Black Rock Series Strata in an Inter-platform Basin: The Lower Carboniferous Datang Formation, Southern Guizhou, Southwest China. *Minerals* 8 (11), 509. doi:10.3390/min8110509

Ding, J. H., Zhang, J. C., Shi, G., Shen, B. J., Tang, X., Yang, Z. H., et al. (2020). Sedimentary Environment and Organic Matter Accumulation for the Longtan Formation Shale in Xuancheng Area. *Acta Sediment. Sin.* 39 (2), 324–340. doi:10.14027/j.issn.1000-0550.2020.056

Ding, J., Zhang, J., Huo, Z., Shen, B., Shi, G., Yang, Z., et al. (2021). Controlling Factors and Formation Models of Organic Matter Accumulation for the Upper Permian Dalong Formation Black Shale in the Lower Yangtze Region, South China: Constraints from Geochemical Evidence. *ACS Omega* 6, 3681–3692. doi:10.1021/acsomega.0c04979

Du, X., Song, X., Zhang, M., Lu, Y., Lu, Y., Chen, P., et al. (2015). Shale Gas Potential of the Lower Permian Gufeng Formation in the Western Area of the Lower Yangtze Platform, China. *Mar. Pet. Geology.* 67, 526–543. doi:10.1016/j.marpetgeo.2015.05.031

Fedo, C. M., Wayne Nesbitt, H., and Young, G. M. (1995). Unraveling the Effects of Potassium Metasomatism in Sedimentary Rocks and Paleosols, with Implications for Paleoweathering Conditions and Provenance. *Geol* 23 (10), 921–924. doi:10.1130/0091-7613(1995)023<0921:uteopm>2.3.co;2

Fu, X. D., Chen, Y. N., Luo, B., Li, W. Z., Zhang, J. Y., Wang, X. F., et al. (2021). Characteristics and Petroleum Geological Significant of the High–Quality Source Rocks in the Gufeng Member of the Middle Permian Maokou Formation in the Northern Sichuan Basin. *Acta Geologica Sinica* 95 (6), 1903–1920. doi:10.1088/1755-1315/600/1/012009

Gallego-Torres, D., Martínez-Ruiz, F., Paytan, A., Jiménez-Espejo, F. J., and Ortega-Huertas, M. (2007). Pliocene–holocene Evolution of Depositional Conditions in the Eastern Mediterranean, Role of Anoxia vs. Productivity at Time of Sapropel Deposition. *Palaeogeogr. Palaeoclimatol. Palaeoecol.* 246 (24), 424–439. doi:10.1016/j.palaeo.2006.10.008

Hatch, J. R., and Leventhal, J. S. (1992). Relationship between Inferred Redox Potential of the Depositional Environment and Geochemistry of the Upper Pennsylvanian (Missourian) Stark Shale Member of the Dennis Limestone, Wabaunsee County, Kansas, U. .*S.A. Chem. Geol.* 99 (1–3), 65–82. doi:10.1016/0009-2541(92)90031-y

Huang, H., Li, R., Jiang, Z., Li, J., and Chen, L. (2020). Investigation of Variation in Shale Gas Adsorption Capacity with Burial Depth: Insights from the Adsorption Potential Theory. *J. Nat. Gas Sci. Eng.* 73, 103043. doi:10.1016/j.jngse.2019.103043

Huang, H., Li, R., Chen, W., Chen, L., Jiang, Z., Xiong, F., et al. (2021). Revisiting Movable Fluid Space in Tight fine-grained Reservoirs: A Case Study from Shahejie Shale in the Bohai Bay Basin, NE China. *J. Pet. Sci. Eng.* 207, 109170. doi:10.1016/j.petrol.2021.109170

Hung, J.-J., Yeh, H.-Y., Peng, S.-H., and Chen, C. T. A. (2018). Influence of Submarine Hydrothermalism on Sulfur and Metal Accumulation in Surface Sediments in the Kueishantao Venting Field off Northeastern Taiwanfluence of Submarine Hydrothermalism on Sulfur and Metal Accumulation in Surface Sediments in the Kueishantao Venting Feld off Northeastern Taiwan. *Mar. Chem.* 198, 88–96. doi:10.1016/j.marchem.2017.12.004

Ibach, L. E. J. (1982). Relationship between Sedimentation Rate and Total Organic Carbon Content in Ancient marine Sediments. *AAPG Bull.* 66, 170–183. doi:10.1306/03b59a5d-16d1-11d7-8645000102c1865d

Jin, Y., Zhang, J., and Shang, Q. (1994). Two Phases of the End–Permian Mass Extinction. *Can. Soc. Petrol. Geol. Memoir.* 17, 813–822.

Kametaka, M., Takebe, M., Nagai, H., Zhu, S., and Takayanagi, Y. (2005). Sedimentary Environments of the Middle Permian Phosphorite-Chert Complex from the Northeastern Yangtze Platform, China; the Gufeng Formation: a continental Shelf Radiolarian Chert. *Sediment. Geology.* 174, 197–222. doi:10.1016/j.sedgeo.2004.12.005

Kennedy, M. J., Löhr, S. C., Fraser, S. A., and Baruch, E. T. (2014). Direct Evidence for Organic Carbon Preservation as clay-organic Nanocomposites in a Devonian Black Shale; from Deposition to Diagenesis. *Earth Planet. Sci. Lett.* 388, 59–70. doi:10.1016/j.epsl.2013.11.044

Kimura, H., and Watanabe, Y. (2001). Oceanic Anoxia at the Precambrian-Cambrian Boundary. *Geol* 29 (11), 995–998. doi:10.1130/0091-7613(2001)029<0995:oaatpc>2.0.co;2

Kun Zhang, K., Jia, C., Song, Y., Jiang, S., Jiang, Z., Wen, M., et al. (2020). Analysis of Lower Cambrian Shale Gas Composition, Source and Accumulation Pattern in Different Tectonic Backgrounds: A Case Study of Weiyuan Block in the Upper Yangtze Region and Xiuwu Basin in the Lower Yangtze Region. *Fuel* 263, 115978. doi:10.1016/j.fuel.2019.115978

Lang, X., Tang, W., Ma, H., and Shen, B. (2020). Local Environmental Variation Obscures the Interpretation of Pyrite Sulfur Isotope Records. *Earth Planet. Sci. Lett.* 533, 116056. doi:10.1016/j.epsl.2019.116056

Large, R. R., Halpin, J. A., Lounejeva, E., Danyushevsky, L. V., Maslennikov, V. V., Gregory, D., et al. (2015). Cycles of Nutrient Trace Elements in the Phanerozoic Ocean. *Gondwana Res.* 28, 1282–1293. doi:10.1016/j.gr.2015.06.004

Liao, Z. W., Hu, W. X., and Cao, J. (2016). A Preliminary Investigation of the Development and Hydrocarbon Potential of the Black Shales in the Upper Permian Dalong Formation, Southern Anhui Province in the Lower Yangze Region, China. *Geol. J. China Universities* 22 (1), 138–151. doi:10.16108/j.issn1006-7493

Liu, Z., and Selby, D. (2021). Deep-water Osmium-Isotope Record of the Permian-Triassic Interval from Niushan, China Reveals Potential Delayed Volcanic Signal post the Mass Extinction. *Glob. Planet. Change* 200, 103473. doi:10.1016/j.gloplacha.2021.103473

Ma, Y. S., Chen, H. D., and Wang, G. L. (2009). *Palaeogeography Atlas for Tectonic-Sequence Lithofacies in South China*. Beijing: Science press.

Mclennan, S. M. (1993). Weathering and Global Denudation. *Journal Geology.* 101 (2), 295–303. doi:10.1086/648222

Metzger, G. J., Greaver, C. A., Jahren, A. H., Smith, A. H., Sheldon, R. M. H., and au, N. D. (2006). Middle-Late Permian Mass Extinction on Land. *Geol. Soc. America Bull.* 118, 1398–1411. doi:10.1130/b26011.1

Montañez, I. P., Tabor, N. J., Niemeier, D., DiMichele, W. A., Frank, T. D., Fielding, C. R., et al. (2007). CO2-forced Climate and Vegetation Instability during Late Paleozoic Deglaciation. *Science* 315, 87–91. doi:10.1126/science.1134207

Mort, H., Jacquat, O., Adatte, T., Steinmann, P., Föllmi, K., Matera, V., et al. (2007). The Cenomanian/Turonian Anoxic Event at the Bonarelli Level in Italy and Spain: Enhanced Productivity And/or Better Preservation? *Cretaceous Res.* 28 (4), 597–612. doi:10.1016/j.cretres.2006.09.003

Murphy, A. E., Sageman, B. B., Hollander, D. J., Lyons, T. W., and Brett, C. E. (2000). Black Shale Deposition and Faunal Overturn in the Devonian Appalachian Basin: Clastic Starvation, Seasonal Water-Column Mixing, and Efficient Biolimiting Nutrient Recycling. *Paleoceanography* 15, 280–291. doi:10.1029/1999pa000445

Murray, R. W., Buchholtz Ten Brink, M. R., Gerlach, D. C., Russ, G. P., and Jones, D. L. (1991). Rare Earth, Major, and Trace Elements in Chert from the

Franciscan Complex and Monterey Group, California: Assessing REE Sources to fine-grained marine Sediments. *Geochimica Et Cosmochimica Acta* 55 (7), 1875–1895. doi:10.1016/0016-7037(91)90030-9

Nesbitt, H. W., and Young, G. M. (1982). Early Proterozoic Climates and Plate Motions Inferred from Major Element Chemistry of Lutites. *Nature* 299, 715–717. doi:10.1038/299715a0

Pedersen, T. F., and Calvert, S. E. (1990). Anoxia vs. Productivity, what Controls the Formation of Organic–Carbon-Rich Sediments and Sedimentary Rocks? *AAPG Bull.* 74, 454–466. doi:10.1306/0c9b232b-1710-11d7-8645000102c1865d

Rimmer, S. M. (2004). Geochemical Paleoredox Indicators in Devonian-Mississippian Black Shales, Central Appalachian Basin (USA). *Chem. Geology.* 206, 373–391. doi:10.1016/j.chemgeo.2003.12.029

Rimmer, S. M., Thompson, J. A., and Goodnight, S. A. (2004). Multiple Controls on the Preservation of Organic Matter in Devonian-Mississippian marine Black Shales, Geochemical and Petrographic Evidence. *Palaeogeogr. Palaeoclimatol. Palaeoecol.* 215 (1–2), 125–154. doi:10.1016/s0031-0182(04)00466-3

Sageman, B. B., Murphy, A. E., and Werne, J. P. (2003). A Tale of Shales, the Relative Roles of Production, Decomposition, and Dilution in the Accumulation of Organic-Rich Strata, Middle-Upper Devonian, Appalachian Basin. *Chem. Geology.* 195 (1), 229–273. doi:10.1016/s0009-2541(02)00397-2

Schenau, S. J., Reichart, G. J., and De Lange, G. J. (2005). Phosphorus Burial as a Function of Paleoproductivity and Redox Conditions in Arabian Sea Sediments. *Geochimica et Cosmochimica Acta* 69, 919–931. doi:10.1016/j.gca.2004.05.044

Schoepfer, S. D., Shen, J., Wei, H., Tyson, R. V., Ingall, E., and Algeo, T. J. (2015). Total Organic Carbon, Organic Phosphorus, and Biogenic Barium Fluxes as Proxies for Paleomarine Productivity. *Earth-Science Rev.* 149, 23–52. doi:10.1016/j.earscirev.2014.08.017

Shanks, W. C., and Bischoff, J. L. (1977). Ore Transport and Deposition in the Red Sea Geothermal System: a Geochemical Model. *Geochimica et Cosmochimica Acta* 41, 1507–1519. doi:10.1016/0016-7037(77)90255-1

Shen, S.-z., Crowley, J. L., Wang, Y., Bowring, S. A., Erwin, D. H., Sadler, P. M., et al. (2011). Calibrating the End-Permian Mass Extinction. *Science* 334 (6061), 1367–1372. doi:10.1126/science.1213454

Slack, J. F., Grenne, T., and Bekker, A. (2007). Suboxic Deep Seawater in the Late Paleoproterozoic, Evidence from Hematitic Chert and Iron Formation Related to Seafloor - Hydrothermal Sulfide Deposits, Central Arizona, USA. *Earth Planet. Sci. Lett.* 255 (1–2), 243–256. doi:10.1016/j.epsl.2006.12.018

Takebe, M., Kametaka, M., Takayanagi, Y., Mimura, K., Sugitani, K., and Yamamoto, K. (2007). Origin and Deposition of Organic Matter in continental Chert of the Middle Permian Gufeng Formation in the Northeastern Yangtze Platform. *Sediment. Geology.* 201, 141–148. doi:10.1016/j.sedgeo.2007.05.011

Taylor, S. R., and McLennan, S. M. (1985). *The Continental Crust: Its Composition and Evolution*. Oxford: Blackwell Scientific Publications, 311.

Tribovillard, N., Algeo, T. J., Baudin, F., and Riboulleau, A. (2012). Analysis of marine Environmental Conditions Based Onmolybdenum-Uranium Covariation-Applications to Mesozoic Paleoceanography. *Chem. Geology.* 324-325, 46–58. doi:10.1016/j.chemgeo.2011.09.009

Tribovillard, N., Algeo, T. J., Lyons, T., and Riboulleau, A. (2006). Trace Metals as Paleoredox and Paleoproductivity Proxies: An Update. *Chem. Geology.* 232, 12–32. doi:10.1016/j.chemgeo.2006.02.012

Tyrrell, T. (1999). The Relative Influences of Nitrogen and Phosphorus on Oceanic Primary Production. *Nature* 400, 523–531. doi:10.1038/22941

Wei, H., Chen, D., Wang, J., Yu, H., and Tucker, M. E. (2012). Organic Accumulation in the Lower Chihsia Formation (Middle Permian) of South China: Constraints from Pyrite Morphology and Multiple Geochemical Proxies. *Palaeogeogr. Palaeoclimatol. Palaeoecol.* 353-355, 73–86. doi:10.1016/j.palaeo.2012.07.005

Wignall, P. B., Sun, Y., Bond, D. P. G., Izon, G., Newton, R. J., Védrine, S., et al. (2009). Volcanism, Mass Extinction, and Carbon Isotope Fluctuations in the Middle Permian of China. *Science* 324, 1179–1182. doi:10.1126/science.1171956

Yao, C., Ma, D., Ding, H., Zhang, X., and Huang, H. (2014). Trace Elements and Stable Isotopic Geochemistry of an Early Cambrian Chert-Phosphorite Unit from the Lower Yurtus Formation of the Sugetbrak Section in the Tarim Basin. *Sci. China Earth Sci.* 57 (3), 454–464. doi:10.1007/s11430-013-4760-9

Young, G. M. (2002). Geochemical Investigation of a Neoproterozoic Glacial Unit: The Mineral Fork Formation in the Wasatch Range, Utah. *GSA Bull.* 114, 387–399. doi:10.1130/0016-7606(2002)114<0387:gioang>2.0.co;2

Zhang, B., Yao, S., Hu, W., Ding, H., Liu, B., and Ren, Y. (2019). Development of a High-Productivity and Anoxic-Euxinic Condition during the Late Guadalupian in the Lower Yangtze Region: Implications for the Mid-capitanian Extinction Event. *Palaeogeogr. Palaeoclimatol. Palaeoecol.* 531, 108630. doi:10.1016/j.palaeo.2018.01.021

Zhang, K., Jiang, S., and Zhao, R. (2022b). Connectivity of Organic Matter Pores in the Lower Silurian Longmaxi Formation Shale, Sichuan Basin, Southern China: Analyses from Helium Ion Microscope and Focused Ion Beam Scanning Electron Microscope. *Geol. J.* 7, 1–13. doi:10.1002/gj.4387

Zhang, K., Song, Y., Jia, C., Jiang, Z., Han, F., Wang, P., et al. (2022a). Formation Mechanism of the Sealing Capacity of the Roof and Floor Strata of marine Organic-Rich Shale and Shale Itself, and its Influence on the Characteristics of Shale Gas and Organic Matter Pore Development. *Mar. Pet. Geology.* 140, 105647. doi:10.1016/j.marpetgeo.2022.105647

Zhang, K., Song, Y., and Jiang, Z. X. (2022c). Quantitative Comparison of Genesis and Pore Structure Characteristics of Siliceous Minerals in marine Shale with Different TOC Contents - A Case Study on the Shale of Lower Silurian Longmaxi Formation in Sichuan Basin, Southern China. *Front. Earth Sci.* 10, 887160. doi:10.3389/feart.2022.887160

Zhang, S. C., Zhang, B. M., and Bian, L. Z. (2005). Development Constraints of marine Source Rocks in China. *Earth Sci. Front.* 12 (3), 39–48.

Zhao, Z. Y., Li, S. J., and Wang, G. H. (2020). Discussion on Sedimentary Environments, Origin and Source of Middle Permian Gufeng Formation Bedded Cherts in the Northern Margin of the Middle–Lower Yangtze Area. *Adv. Earth Sci.* 35 (2), 137–153. doi:10.11867/j.issn.1001-8166.2020.003

Zhou, X., Chen, D., Qing, H., Qian, Y., and Wang, D. (2014). Submarine Silica-Rich Hydrothermal Activity during the Earliest Cambrian in the Tarim Basin, Northwest China. *Int. Geology. Rev.* 56 (15), 1906–1918. doi:10.1080/00206814.2014.968885

Conflict of Interest: The authors declare that the research was conducted in the absence of any commercial or financial relationships that could be construed as a potential conflict of interest.